International Journal of Hydrogen Energy 69 (2024) 586–607

Contents lists available at ScienceDirect

International Journal of Hydrogen Energy

journal homepage: www.elsevier.com/locate/he

Experimental study and numerical simulation on porosity dependent direct reducibility of high-grade iron oxide pellets in hydrogen

Behzad Sadeghi [a,*], Pasquale Cavaliere [a,**], Mutlucan Bayat [a], Niloofar Ebrahimzadeh Esfahani [b,c], Aleksandra Laska [d], Damian Koszelow [e]

[a] Department of Innovation Engineering, University of Salento, Via per Arnesano, 73100, Lecce, Italy
[b] Faculty of Electrical Engineering and Information, Slovak University of Technology, Ilkovicova 3, 81219, Bratislava, Slovakia
[c] Omnics Research Group, Department of Mathematics and Physics University of Salento, CNR-Institute of Nanotechnology, INFN Sezione di Lecce, Via per Monteroni, 73100, Lecce, Italy
[d] Faculty of Mechanical Engineering and Ship Technology, Gdansk University of Technology, Narutowicza 11/12, 80- 233, Gdansk, Poland
[e] Advanced Materials Centre, Faculty of Electronics, Telecommunications and Informatics, Gdansk University of Technology, 80-233, Gdansk, Poland

ARTICLE INFO

Keywords:
Hydrogen-based direct reduction
Numerical
Simulation
High grade
Iron oxide pellets

ABSTRACT

The transition to more environmentally friendly steel production methods has intensified research into hydrogen-based direct reduction (HyDR) of iron oxide pellets. The aim of this study is to systematically investigate the kinetics of the reduction process, the evolution of porosity and the resulting microstructural changes on the reduction behavior of high-quality pellets during HyDR of iron ore at different temperatures. A modified mathematical model is developed based on the shrinkage kernel model, taking into account both mass and heat transport in a hydrogen atmosphere. The effects of temperature, particle size and time on the reduction behavior of the pellets are investigated. The simulated results are validated and discussed by the results of a batch of iron oxide pellets consisting of ten almost spherical pellets subjected to the direct reduction process with pure hydrogen. The results show that the total energy input to the HyDR process is a complex balance of factors, including chemical reaction rates, diffusion dynamics and entropy generation. The increase in free volume and simultaneous decrease in pore diameter reflect the dynamic nature of the microstructure, which includes additional free volume and defects due to the volume discrepancies and associated stresses between the reactant and product phases. Furthermore, the data show that higher temperatures accelerate the reduction reactions, especially the transformation of wustite into metallic iron. This phase transition is characterized by a significant volume change that cannot be accommodated by elastic deformation alone, leading to the development of lattice defects such as cracks, creep pores and dislocations that serve as stress relief mechanisms. The trends for porosity change at 950 °C and 1000 °C observed in the experimental results are correct and in good agreement with the numerical and simulated results.

1. Introduction

Iron production is a crucial step in the manufacture of iron and steel. It involves the conversion of iron ore into molten iron through a series of chemical reactions. The current annual consumption of iron ore for this process amounts to 2.3 billion tons, from which about 1.32 billion tons of pig iron are extracted [1–3]. This concern is a top priority for the industry, as more than 70% of the world's iron production currently takes place via a blast furnace and a downstream oxygen converter [4]. In reality, such a large amount of CO_2 production contradicts the goals of achieving low-carbon steel production and reducing CO_2emissions by over 80% by 2050 [5–7]. An alternative approach to large-scale and sustainable iron oxide reduction is hydrogen-based direct reduction (HyDR) of iron oxide, which is attracting a lot of attention in the iron and steel industry as one of the most promising solutions in this context [4,8,9]. The most common burden materials were used for the direct-reduced iron (DRI) process, are pellets that generally containing pre-porosities with different size and the surface area.

The process of iron production is essentially complex and involves various stages, each of which has its own characteristics and

* Corresponding author.
** Corresponding author.
E-mail addresses: behzad.sadeghi@unisalento.it (B. Sadeghi), pasquale.cavaliere@unisalento.it (P. Cavaliere).

https://doi.org/10.1016/j.ijhydene.2024.05.050
Received 15 March 2024; Received in revised form 18 April 2024; Accepted 4 May 2024
Available online 9 May 2024

requirements. An important aspect of iron production is the porosity of the starting material, such as iron oxide ore and pellets. Porosity, i.e. the presence of open spaces or voids in the material, plays an important role in determining the efficiency and quality of the ironmaking process. Iron ore pellets, on the other hand, are a manufactured product that is used as a feedstock for iron production. Pellets are produced in the pelletizing process by agglomerating fine iron ore particles into small, spherical balls, which inevitably creates porosity [10,11]. In the context of ironmaking, porosity refers to the presence of voids or pores in the feedstock materials, such as iron oxide ore and pellets. Porous pellets allow for better gas–solid reduction behavior, which promotes the transport of heat and mass during ironmaking reactions [12].

This leads to faster reaction rates and improved overall process efficiency. In addition, the porosity of the iron oxide pellets has an effect on the mechanical strength of the materials, which is important for handling and transportation. Porosity plays a crucial role in direct reduction as it has a direct impact on the efficiency and productivity of the process, i.e. on the reduction rate, the gas-solid reactions and the gas transport within the reactor [11,13]. In gas–solid reduction reactions, high porosity facilitates the diffusion of gas molecules and further promotes the reduction reactions [12]. In other words, the reduction time correlates with the absolute porosity and the size of the surface pores. Larger pores lead to a faster reduction, depending on the density of the pellet, with a higher density leading to a longer reduction time [14,15]. In this context, previous literature has documented that the microstructural elements and the impurities dissolved in the pellets can have significant effects on the HyDR behavior of iron oxide pellets and influence the microstructural changes during reduction, the pore size distribution and the overall reduction kinetics [14,16,17]. Cavaliere et al. [14,15,18], studied the hydrogen direct reduction and processing parameters on the reduction behavior of high-quality pellets and showed a remarkable increase in porosity when the pellets are fully metallized. They also showed that the pore size and the tortuosity of the pores increase as the hydrogen reduction progresses. The presence of various impurities and intermediate iron oxide variants can also influence the nano/microstructure and chemistry of the resulting iron, which can affect its properties and quality [17].

In an industrial reactor for the DR process, the movement of the oxide pellets leads to changes in the chemical potentials of the gaseous species and the temperature. These fluctuations are caused by the interaction between the pellets and the injected gas mixture. In addition, the chemical potentials of the species within the individual pellets can differ at a certain position [19]. These variations can be caused by factors such as the composition and structure of the pellet itself as well as the local conditions in the reactor. It is therefore necessary to understand these variations in chemical potentials. Temperature is critical for optimizing reactor performance and ensuring efficient processing of the oxide pellets. In addition, the process of reducing the pellets with gasses involves three main phases [2,19]. In the gas phase, a mass transfer takes place first, i.e. the movement of the gasses within the reactor. This interaction between the gas mixture and the sintered pellets facilitates the efficient transfer of reactants and products, and the effectiveness of this mass transfer is critical to the overall reduction reaction. Once the gasses have come into contact with the sintered pellets, they must flow through the product layer surrounding the pellets. This layer, which consists of reaction products from the reduction process, requires efficient mass transfer so that the reactants can reach the oxide interface for the subsequent chemical reactions. The chemical reactions that make up the reduction reaction ultimately take place at the interface between the product layer and the oxide pellets. Factors such as temperature and time of reduction, gas composition and the properties of the pellets influence these reactions. To achieve a successful reduction of sintered pellets by gasses, it is crucial to understand and optimize these main steps. To fully understand the behavior of pellet reduction and to enable efficient dynamic control, it is therefore essential to develop an accurate mathematical model that describes the intrinsic properties of the pellet.

There is modeling work for the reduction of single pellets by different mechanisms and for multi-particle reduction processes [20–28]. In general, three primary mathematical models have been used to model pellet reduction: the non-reacting shrinking core model with one interface, the non-reacting shrinking core model with three interfaces, and the porous solid model (also known as the grain model). In a paper by Bonalde et al. [28], the grain model describes the reduction kinetics of iron ore pellets. The model with an interface was a fundamental mathematical model based on the chemical reaction of iron and wustite (W) at the interface and incorporated Fick's law to determine the mass transfer of gas species within the pellet [29,30]. The behavior of gas transfer in the porosities as a control step of the overall reduction process was described according to the previously published literature. The investigation of the influence of pellet diameter and porosity on the reduction showed that increasing the porosity accelerates the diffusion of the gas species, which leads to a faster reduction process [14,31]. In addition, the size of the pores decreases from the larger pellet to the middle one, only to increase again in the pellet with the smallest diameter [10]. On the one hand, the differences in the physical and chemical properties of iron ore pellets and, on the other hand, the kinetic parameters such as time and temperature considerably limit the applicability of existing process models to different types of pellets and experimental conditions. Therefore, a mathematical model that takes into account the exact structural details of the pellet for the direct reduction of iron oxide pellets must include the type of physical properties, reduction time and local temperature. The current approach provides a solid basis for dynamic modeling of the pellet reduction process, but further efforts are certainly needed to create a realistic process model.

Considering the different steps involved in the reduction of pellets by gasses, the development of a process model requires a careful identification of the reduction mechanisms. To develop an effective process model, it is critical to examine the intricacies of the individual steps and how they interact. By carefully identifying and characterizing the reduction mechanisms and the gas behavior in the pre-porosities, the process model can accurately represent the complex dynamics of the reduction process. In addition, the process model should take into account the variations in temperature, time and the properties of the oxide material. These factors significantly influence the reduction mechanisms and must be included in the model to ensure its accuracy and reliability. The development of a process model that takes into account the different steps in the reduction of sintered pellets by gasses therefore requires a comprehensive understanding of the underlying mechanisms.

Besides all the advantages that the developed models have in the field of direct reduction of iron ore pellets, the lack of consideration of the initial geometry of the starting pellet, which can lead to various non-uniformities in terms of temperature distribution, the behavior of the gas in the pores as well as the active mass transfer of the materials during the reduction process, can be mentioned as the most important obstacle and dilemma of these models. In this context, Qiu et al. [29,30] have recently shown that the gas behavior in terms of velocity and pressure within the pores of a pellet can be anisotropic and strongly depends on the properties of the pores. In this context, this article aims to investigate the crucial role of porosity on the reducibility behavior of iron oxide rock through a combined approach based on experimental data and numerical simulations of a real porous pellet based on X-ray computed tomography images. The development and evolution of both qualitative and quantitative porosity and the effective role of this parameter on the mechanisms involved in the process of direct reduction of iron ore pellets are closely monitored and discussed in detail. In the present study, a modified mathematical model is developed based on the model of the shrinkage core, taking into account both mass and heat transport in a hydrogen atmosphere. The effects of temperature, particle size, time and porosity on the reduction behavior of pellets are investigated. The simulated results are validated and discussed using the results of a batch of iron oxide pellets consisting of 10 nearly spherical pellets subjected to

the direct reduction process with pure hydrogen. In the present work, the high-level pellet tomography images were simulated with the finite element method (FEM) using COMSOL Multiphysics software to obtain detailed insights into the complex physical phenomena governing the process, including porosity coalescence caused by the reduction, gas flow and heat transfer within the pellets, reaction kinetics and gas-solid interactions.

2. Experimental section

Reduction experiments were carried out with the pellet samples provided by VALE (Brazil). The main mineral phase of the pellet was hematite, Fe_2O_3, (H) and a small amount of magnetite, Fe_3O_4, (M) and quartz, as indicated in Table 1.

The pellets analyzed in the present study were provided by VALE (Brazil); the production process of the pellets is described in detail in Ref. [14]. The selected pellets had a good spherical shape with an average diameter in the range of 1–2 cm (Fig. 1(a)), a density of 3600–5200 kg/m^3 and a specific surface area of 1500–1600 cm^2/g. The density of the pellets was determined by measuring seven diameters of the pellets. After calculating the average diameter of the pellets, these were used to calculate the density after the pellets were weighed with a precision balance. The pellet reduction experiments were carried out in a self-designed and developed shaft furnace (Fig. 1(b)).

The experiments on direct reduction were carried out in the temperature range 950–1000 °C. The gas composition was high-purity hydrogen (99.99 pct) at pressures of 1–8 bar. The flow rate of the reducing gas was 0.5 L/min and the basicity index (referred to as CaO/SiO_2 ratio) was between 0 and 2.15. Pure hydrogen was used to isolate its effects on reducibility and microstructural changes, eliminating variables from impurities. This selection acts as a standard for future comparisons. The flow rate of 0.5 L/min, chosen based on initial tests and literature [32,33] ensures thorough reduction and aligns with industrial practices for applicability. Three tests were performed for each condition to ensure reproducibility of the results. The pore aspect and the evolution of the pellet were analyzed by microtomography using Phoenix v/tome/x s (General Electric). X-ray computed microtomography is a non-destructive technique that allows the internal and three-dimensional visualization of a sample exposed to ionizing radiation without the need for physical or chemical preparation of the pellet. It is based on the same principles as conventional radiography, in which each part of a sample absorbs the rays differently. In this way, it is possible to examine two-dimensional cross-sections non-destructively and reconstruct them through mathematical principles to create the corresponding three-dimensional model of the sample, which allows the visualization and quantification of the internal structure of the material. Computed tomography produces an image that is very close to reality by displaying the average attenuation of each small-volume element, organizing the beam attenuation information and quantifying the information [14,34,35]. The segmentation of the pores was performed with the free software FIJI/ImageJ. A lower limit was set visually, where some pores were not selected, and an upper limit, where pores that were not yet filled could be selected. The threshold (maximum or minimum) was set for all sample layers. The determination of the threshold value is important as it has a significant influence on the determination of the porosity percentage of iron ore pellets [14]. The degree of reduction, R_{ex}, is defined by Ref. [19] as follows,

$$R_{ex} = \frac{W_0 - W_t}{W_0 - W_\infty}$$

Where W_0, W_t and W_∞ are the initial weight of the pellet, the weight of the pellet at time t, and the theoretical weight after complete reduction, respectively. The details of the experiment have been described in previous publications by our group [10,14,36]. Since the kinetics of the direct reduction process is directly influenced by the properties of the reducing gas (temperature, pressure and type of gas), the temperature and time of reduction and the physical properties of the pellet (diameter, density, porosity and tortuosity), there are two different modes. In this context, a HyDR process for pellets is considered. In the first case, we only considered the temperature and time changes in the evolution of porosity and tortuosity (unreduced state). In the second case, the role of the reducing gas on the evolution of porosity and tortuosity was investigated at the same temperature and time as before (reduced state).

3. Numerical approach

Numerical modeling of the reduction processes plays a central role in deciphering the complex transformation of H into iron, which involves a sequence of reactions: H (H) → M (M) → Wustite (W) → Iron (Fe).

In this section, a model is presented that focuses on the evolution of the physical properties of the pellets during the DRI process (Fig. 2). It was specifically developed to decipher the intricate interplay of parameters that control the reducibility of H pellets. Of greatest importance are the dynamic changes in the evolution of porosity and tortuosity during the reduction phases, which influence the course of the individual reactions. In this context, reducibility is an important parameter that quantifies the degree of conversion of H to iron during the reduction reactions. In the following sections, we focus on the detailed structure of our model and emphasize the indispensable role of porosity evolution and changes in tortuosity. This paper deals with the meaning of the individual terms, explains the reasons for the choice of parameters and their respective exponents, and highlights the complicated dynamics of the HyDR process.

Studies have shown that porosity and pore size develop as a function of the reduction temperature, which underlines their importance for the process [10]. In contrast, tortuosity, which characterizes the path of particles through a medium, is also a decisive factor [14,18]. The relationship between porosity, tortuosity and permeability is of fundamental importance because tortuosity influences the flow behavior through porous media and thus affects the overall efficiency of the direct reduction process. Therefore, understanding and quantifying the importance of porosity and tortuosity is essential for optimizing the direct reduction process and predicting the behavior of iron oxide pellets during the direct reduction process. To better understand how porosity and tortuosity evolve during the direct reduction process, it is necessary to investigate the influence of temperature and time on these factors prior to HyDR.

The reduction of Fe2O3 does not occur directly to metallic Fe. If the reduction temperature is below 570 °C, the reduction to Fe occurs gradually from Fe2O3 to Fe3O4 and further to Fe. At reduction temperatures of more than 570 °C, on the other hand, the reduction takes place from Fe2O3 via Fe3O4 to Fe(1-x)O and then on to Fe. In the simplest and most widely accepted model in the literature [37–39], the HyDR process is characterized by a hierarchy of phenomena that can influence the reaction at different lengths and time scales [14,40], as shown in Fig. 3. This process begins with a chemical reaction on the outer surface of the pellet with hydrogen gas and continues with the diffusion of hydrogen into the porous iron layer that develops towards the interior of the pellet to reach the interface between Fe and Fe(1-x)O

Table 1
The chemical compositions of the pellets (all values are in wt. Percent).

TFe (%)	Fe_2O_3%	CaO (%)	Mn (%)	Al_2O_3 (%)	SiO_2 (%)	P (%)	MgO (%)	S (%)
67.24	96.63	1.02	0.144	0.38	1.97	0.031	0.63	0.018

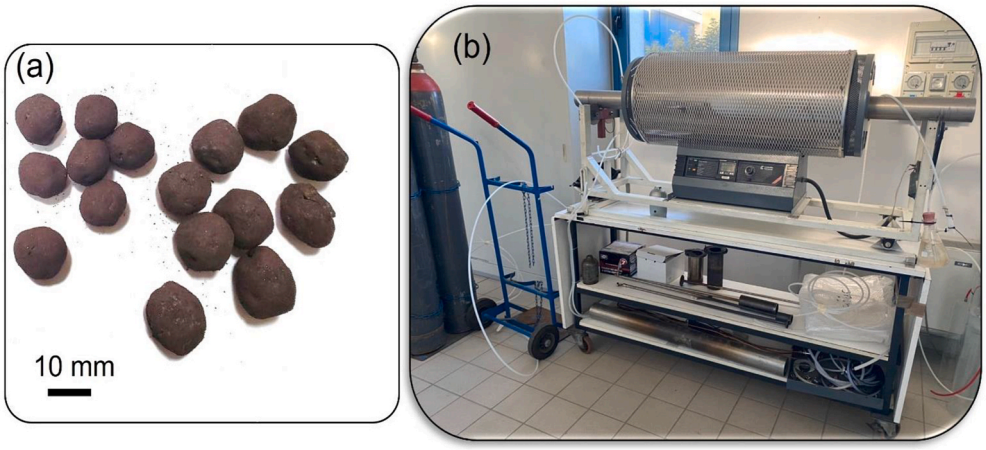

Fig. 1. (a) Pellets employed in the present study (b) Self-designed shaft furnace.

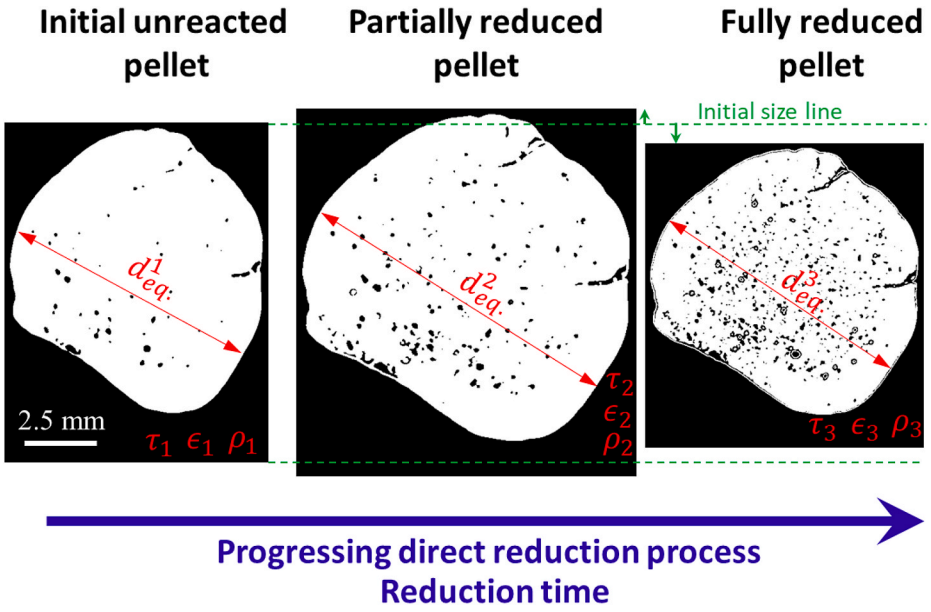

Fig. 2. Reaction process in progressive conversion mode based on shrinking core/particle model. $d_{ed.}$, τ, ϵ, and ρ are the equivalent diameter, tortuosity, porosity and density of pellet. The green dashed line indicates the change in diameter in at least one direction. (For interpretation of the references to color in this figure legend, the reader is referred to the Web version of this article.)

and produce iron and water. The part of the gas that is on its way to the center of the pellet diffuses into the Fe(1-x)O layer to reach the Fe(1-x)O/Fe3O4 interface, which in turn causes the reduction of M to Fe(1-x)O. Finally, the remaining hydrogen gas diffuses into the M layer to reach the M-M interface. In this step, H is reduced to M to complete the reduction reaction. It can be concluded that various phase transformations, mass transfer and mechanical interactions take place throughout the process, which together lead to the development of the reduction process.

The pellet mesh is shown in Fig. 4, which contains between 170,000 and 200,000 (plus 55000–60000 internal degrees of freedom) triangular cells for different geometries. Direct reduction with hydrogen reveals complex physico-chemical-mechanical interactions leading to very complex reduction mechanisms characterized by continuous steps in terms of mass transport and volume changes. Chemical non-catalytic solid-gas reactions involve heat transfer, mass transfer, chemical reactions, changes in physical properties, etc [40–42]. In other words, the reduction of pellets by a gas must take place in the following process steps: Mass transfer in the gas phase, mass transfer within the solid product layer, chemical reaction between the reducing agent and the solid oxide, formation of water vapor and carbon dioxide, iron oxides and iron, diffusion of the reaction products in the solid state and diffusion of the gaseous products back to the pellet surface [15,30]. This dynamic behavior leads to complications in the precise analytical analysis of the entire reduction process. The main hypotheses proposed to simplify the process are therefore as follows.

- Both the gas and solid phases are considered continuous, and the gas phase obeys the ideal gas law.
- The density of the gas is constant
- The reactions are reversible: first-order and proceed topochemically.

4. Reduction kinetic

4.1. Evolution of pellet porosity and tortuosity

Porosity and tortuosity are crucial parameters in the HyDR process that significantly influence the performance and properties of iron oxide

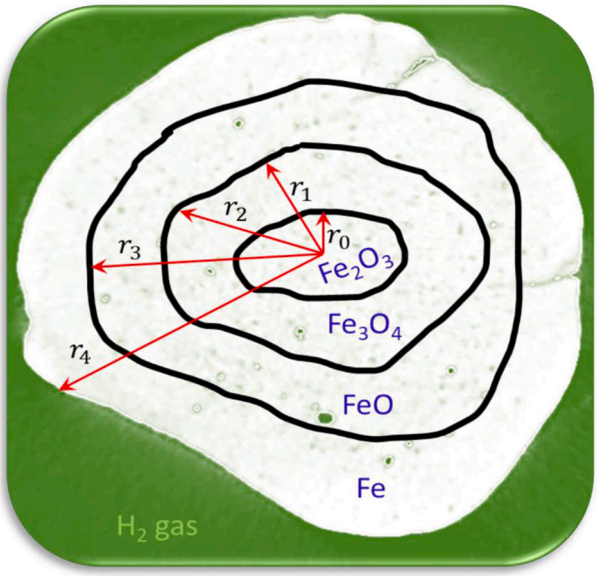

Fig. 3. The three-layer model of the unreacted shrinking core shows the product layers Fe3O4, FeO, and Fe as well as the H core Fe2O3. Each particle was surrounded by an atmosphere of H_2-gas.

pellets. Porosity plays a crucial role in facilitating gas penetration, increasing reaction rate and improving reduction performance. It influences gas diffusion, permeability and overall reduction kinetics by providing pathways for efficient gas flow and reaction sites. Conversely, tortuosity has a negative effect on gas diffusion, leading to slower rates and lower efficiency due to longer path lengths and obstacles. It also affects permeability, hinders gas flow and causes uneven distribution within the pellet structure, leading to localized reactions and lower rates. Overall, both porosity and tortuosity influence the effective utilization of the reduction gas and thus determine the success of the reduction process.

4.2. Unreduced state

Time and temperature play an important role in the palletization and direct reduction of iron oxide pellets. In connection with palletizing, temperature and time have a considerable influence on the physical and chemical transformations of the iron ore particles. Studies [14,18,36,43–45] have shown that the reduction temperature has a considerable influence on the extent of reduction in the direct reduction of iron oxide pellets. The temperature profiles and the temperature within the particles during the reduction process show the dynamic characteristics of temperature changes, which directly affect the reduction kinetics and the development of the pellet microstructure.

According to the literature [43,46,47], in palletization process the porosity rate $\left(\frac{d\varnothing}{dt}\right)_{Pel.}$ can be expressed as

$$\left(\frac{d\varnothing}{dt}\right)_{Pel.} = k \times \varnothing^{n} \times e^{(E/T)} \times t^{m} \times \frac{1}{\tau^{p}} \times \frac{1}{\dot{\tau}^{q}} \quad (1)$$

Where k, n, m, p, and q are the rate constants for the palletization process, an empirical constant related to the influence of porosity on the

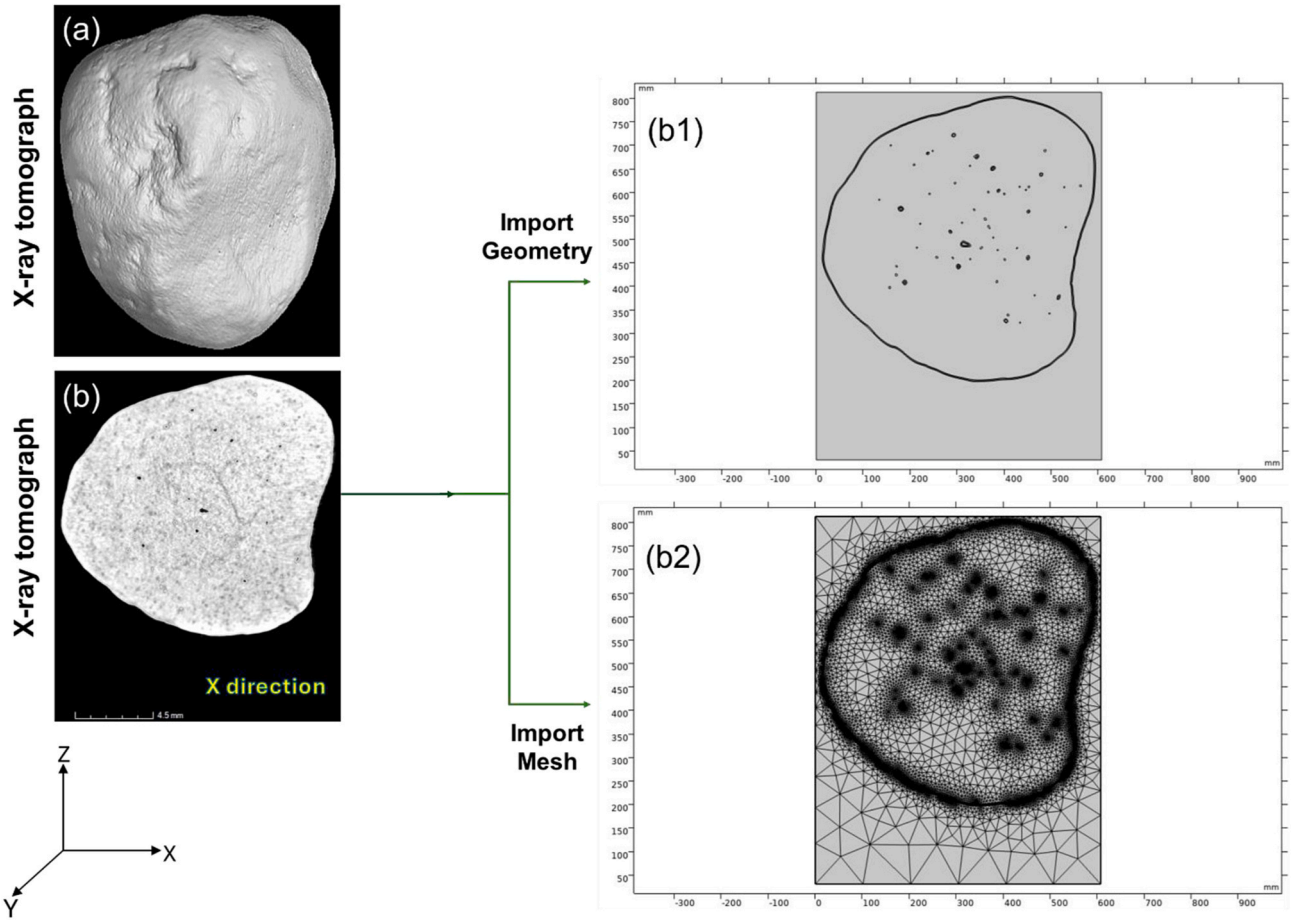

Fig. 4. Image processing steps: (a) original X-ray tomography image, (b) cross-sectional view with internal porosity in the X-direction, (b1) imported geometry, and (b2) corresponding tetrahedral meshing.

porosity rate, and an empirical constant related to the influence of time on the porosity rate, and empirical constant related to the influence of tortuosity on the porosity rate, respectively. ∅ and τ are the percentage of porosity and the tortuosity, while $\dot{\tau}$ is the tortuosity rate calculated from the derivative of the tortuosity with respect to time (Table 1S). E is the activation energy (~477,*kJ-mol.* [14]) and R is the gas constant (8.314,*J-mol.K.*). T is the temperature in Kelvin, and t is the time. All of these constants can be determined by nonlinear fitting in MATLAB using our experimental or simulation data. Table 2 lists the calculated values of all constants.

In order to calculate the porosity (∅) is calculated by

$$\varnothing = \frac{V_p}{V_{cell}} \tag{2}$$

Where V_p and V_{cell} are the pore volume and the total volume of the pellet, respectively. Tortuosity is the actual path length (L) through a porous medium with a straight-line or Euclidean distance ($L_{Eu.}$) that would be traveled in the absence of obstacles [48]. In addition, to calculate the tortuosity value, the X-ray computed tomography images were first binarized, and then the tortuosity was calculated based on the GR algorithm in the Fiji-ImageJ software. In addition, the porosity of a particle is defined as the ratio between the pore volume and the particle volume, and radius of a sphere with the same volume as the irregular object [30]. The calculated porosity values are the average porosity values in the X, Y, and Z sections based on the values obtained from the Gaussian fit of the porosity-size-frequency diagram generated using the Fiji-ImageJ software. It is worth noting that the porosity and tortuosity factors are specific characteristics of each type of pellet and are independent of the gas properties.

4.3. Reduced state

The pores in an iron ore depend on the duration of the reduction reaction, so that intermediate pores can form during the gradual reduction of iron ore. Moreover, the surface of the particles is usually not smooth and continuous but rough, and the particles may have internal cracks and become porous. In addition, in most pellets used as porous media, pores with different diameters are twisted and interconnected, and the path for diffusion of gas molecules within the pores is tortuous. Therefore, a transport mechanism considering all kinds of transport modes such as molecular diffusion, and Knudsen diffusion can be calculated by a D_i^{eff} for each gaseous species considering the total effective intraparticle diffusion as follows [49]:

$$D_{eff} = \frac{\varnothing}{\tau} D_i \tag{3}$$

In fact, $\frac{\varnothing}{\tau}$ is known as a porous media factor.

D_i can be expressed as follows:

$$\frac{1}{D_i} \cong \frac{1}{\mathrm{D_{iK}}} + \frac{1}{\mathrm{D_{ij}}} \tag{4}$$

Where D_{ij} and D_{iK} are the coefficient of molecular diffusion and Knudsen diffusion, respectively.

The D_{iK} is considered depending on the pore diameter of the porous pellet, measured in m^2/s and it can be calculated as

$$\mathrm{D_{iK}} = 1.054 \,.\, \mathrm{d_p} \,.\, \sqrt{\frac{8RT}{\pi M_i}} \tag{5}$$

Table 2
The constants calculated using Eq. (1).

k	n	m	p	q
6.98	−0.29 ± 0.08	−0.95 ± 0.11	0.0091 ± 0.001	0.0054 ± 0.006

Where d_p, and M_i are the mean pore size of the porous media and the molecular weight of H_2 gas. Temperature (T) has units of K, and R is gas universal constant (8.314 J/mol.K).

Binary molecular diffusion (D_{ij}) is determined by the Fuller-Schettler-Giddings (FSG) correlation and can be defined as in [39,50]

$$\mathrm{D_{ij}} = \frac{0.00143.\ \mathrm{T}^{1.75}}{\mathrm{P_b.MW_{ij}^{1/2}}.\left(\left(\mathrm{V_i^{\frac{1}{3}}} + \mathrm{V_j^{\frac{1}{3}}}\right)\right)^2} \tag{6}$$

$$\mathrm{MW_{ij}} = \left[\frac{1}{\mathrm{MW_i}} + \frac{1}{\mathrm{MW_j}}\right]^{-1} \tag{7}$$

Where P_b (1 and 5 bar), MW_{H2} (~ 2 g/mol), MW_{H2O} (18 g/mol), V_{H2} (7.07 cm^3/mol [51]), and V_{H2O} (12.7 cm3/mol [51]) are the pressure, the molecular weight of H_2 and H_2O, and the diffusion volume of H_2 and H_2O, respectively. From binarized images and calculating the frequency diagram and the size distribution of the pores, the different equivalent radii of the pores within the pellet contain three categories namely, 1–7 μm(average ~ 4 μm, this average value was taken from small pellets reduced at 950 and 1000 °*C*), 8–20 μm (average ~ 14 μm, this average value was taken from medium pellets reduced at 950 and 1000 °*C*), and 21–50 μm (average ~ 36.72 μm, this average value was taken from big pellets reduced at 950 and 1000 °*C*). The values for the D_{ij} and D_{iK} are calculated based on the relevant equations and given in Table 3.

Table 4 shows the calculated effective diffusion coefficients for each pellet during HyDR. It should be noted that the values of ∅ and $\boldsymbol{\tau}$ were calculated for different situations and given in Table 2S.

All images extracted from the Fiji ImageJ software can be found in the supplementary material. Relating porosity, the rate of porosity evolution ($\frac{d\varnothing}{dt}$) and tortuosity (τ) directly can be challenging, as these parameters depend on various factors and their relationships can be complex. Consider these basic concepts, such as 1- as porosity increases, tortuosity tends to increase as there are more pathways for diffusion, making the overall pathway more tortuous; 2- the rate of porosity development can indirectly affect tortuosity. If porosity develops rapidly, it could affect the overall structure and tortuosity.

The total porosity rate is made up of three hierarchical porosity rates, namely $\left(\frac{d\varnothing}{dt}\right)_{H\to M}$, $\left(\frac{d\varnothing}{dt}\right)_{M\to W}$, and $\left(\frac{d\varnothing}{dt}\right)_{W\to Fe}$.

$$\frac{d\varnothing}{dt} = \left(\frac{d\varnothing}{dt}\right)_{H\to M} + \left(\frac{d\varnothing}{dt}\right)_{M\to W} + \left(\frac{d\varnothing}{dt}\right)_{W\to Fe} \tag{8}$$

According to the modified volume reaction model developed by Ghalandari et al. [52],

$$\frac{d\varnothing}{dt} = 1 \Big/ V_p\rho_p(R_{H\to M} + R_{M\to W} + R_{W\to Fe}) \tag{9}$$

Where V_p, and ρ_p are the initial density and initial pellet volume.

Taking into account the changing density in each layer, the effective diffusion coefficient of the porous particle was determined by considering the morphology of the particle, which in turn influenced the

Table 3
Coefficient values of molecular diffusion and Knudsen diffusion as a function of pore size at 1 bar pressure.

		950 °*C*	1000 °*C*
D_{ij} (m^2/s)		14.90	15.99
D_{iK} (m^2/s)	small	~479 × 10^{-6}	~489 × 10^{-6}
	medium	~1679 × 10^{-6}	~1713 × 10^{-6}
	big	~4404 × 10^{-6}	~ 4493 × 10^{-6}
D_i'	small	~ 14.45 × 10^{-6}	~15.48 × 10^{-6}
	medium	~14.76 × 10^{-6}	~15.84 × 10^{-6}
	big	~14.84 × 10^{-6}	~15.93 × 10^{-6}

Table 4
The **effective total diffusion coefficient** ($cm^2.s^{-1}$) as function of pellet size at 950 °C and 1000 °C.

Pellet	950	1000
small	9.69×10^{-3}	5.53×10^{-3}
medium	9.77×10^{-3}	8.85×10^{-5}
big	1.52×10^{-5}	5.77×10^{-5}

density. Therefore, considering the density changes for each phase and the tortuosity, equation (8) can be rearranged as follows:

$$\frac{d\varnothing}{dt} = \left(\frac{M_H R_{H\to M}}{V_{p,H}\rho_{eff.,H}} + \frac{M_M R_{M\to W}}{V_{p,M}\rho_{eff.,M}} + \frac{M_W R_{W\to Fe}}{V_{p,W}\rho_{eff.,W}}\right) \tag{10}$$

Where the ρ_{eff} and V_p the effective density and pore volume. $R_{H\to M}$, $R_{M\to W}$, and $R_{W\to Fe}$ are the reaction rate of H to M, M to wustite, and wustite to iron, respectively.

In addition, the effective density of the H ($\rho_{eff.,H}$) can be defined as

$$\rho_{eff.,H} = (1 - \varnothing)\rho_{pure,H} \tag{11}$$

Where $\rho_{perfect,H}$ is the perfect particle density of the pellet wthout voids. The approximate pure densities (ρ_{pure}) of iron oxides are as follows: Fe_2O_3 or H has a density of approximately 5.24 g/cm^3, Fe_3O_4 or M has a density of approximately 5.17 g/cm^3, and FeO or wustite has a density of approximately 5.70 g/cm^3. The other product layers are also determined by the effective density of the reactant layer multiplied by the mass equivalent as follows:

$$\rho_{eff.,M} = \rho_{eff.,H}\, q_{m,H} \tag{12}$$

$$\rho_{eff.,W} = \rho_{eff.,M}\, q_{m,M} \tag{13}$$

Here $q_{C,A}$ stands for the mass equivalence which represents the mass of the product C for every consumption of A [37]. Knowledge of this point is necessary because diffusion is a key mechanism for the transport of species through interconnected pores during the sintering of porous materials. By defining the D_i^{eff} which takes into account different factors such as porosity, tortuosity and different diffusion modes, it is possible to correlate the mass transport and the evolution of porosity during the HyDR process. By introducing the effective diffusion coefficient into the porosity rate equation, it is assumed that the rate of porosity change is influenced by diffusion phenomena in porous media. The justification for this approach lies in the idea that the change in porosity over time is influenced by these diffusion characteristics, as the diffusion of species through the porous medium becomes more complicated due to factors such as porosity and tortuosity. Therefore, the D_i^{eff} can be included in eq. (10);

$$\frac{d\varnothing}{dt} = \left(\frac{M_H R_{H\to M}}{V_{p,H}\rho_{eff.,H}} + \frac{M_M R_{M\to W}}{V_{p,M}\rho_{eff.,M}} + \frac{M_W R_{W\to Fe}}{V_{p,W}\rho_{eff.,W}}\right).\, D_{eff} \tag{14}$$

It is worth noting that the values of density changes for different phases at different temperatures are on the order of micron scale, which is the reason why the density values are in more than five decimal places.

Considering the molecular weights (M) of Fe_2O_3:159.69 g/mol, Fe_3O_4:231.535 g/mol, and FeO: 71.845 g/mol, the porosity rate can be estimated by eq. (9). The rate of each reaction was estimated from the experimental results. Fig. 3 shows the reduction degree of reduction and the rate of reduction as a function of time at 950 °C and 1000 °C. Based on the experimentally observed reduction kinetics in terms of the reduction degree for the HyDR of commercial H pellets [2] and the HSC estimates for the evolution of the kinetic behavior and the reduced equilibrium amount [53,54], it can be concluded that the reduction rates of the first two average reduction rates, i.e. Fe2O3 to Fe3O4 and Fe3O4 to FeO, are extremely high, while they become much slower for the reduction of FeO to Fe [1]. It should be noted that most of the proposed models and experimental data have shown that the time required for the first, second, and third reactions is closely correlated with the pellet size, temperature, and other parameters. Therefore, based on the experimental and modeled results [1,2,19,30], the time required (Δt) required for the reduction of Fe2O3 to Fe3O4, followed by the reduction of Fe3O4 to FeO, and finally, the reduction of FeO to Fe is estimated differently for each intermediate reaction and pellet size in this work. According to our database and preliminary experimental results, the maximum times required for the reduction of Fe2O3 to Fe3O4, Fe3O4 to FeO, and FeO to Fe are approximately 2–5 min, 5–30 min, and 30–90 min, respectively.

In addition, the HyDR process is known as a hierarchy of phenomena that can influence various reactions from transport and reaction kinetics to chemical reactions that occur on different length and time scales. It is therefore to be expected that changes can be observed in the curve of reaction rate versus time (Fig. 5), which can be explained by the kinetic and thermodynamic differences of the reactions [2,11,55,56]. However, due to the strong dependence of the reaction rate on temperature, the regions related to the individual phase partially overlap at higher reduction temperatures. Therefore, in this study, an attempt was made to estimate the average reaction rate for each intermediate reaction using the plots shown in Fig. 6. It shows the dependence of the reaction rate on the degree of reduction and time for different sizes of H pellets at 950 °C and 1000 °C. The calculated values are given in Table 5.

Figs. 7–9 show microtomographic images of small, medium and large pellets, respectively, showing their pore aspects and development in both unreduced and reduced states after exposure to HyDR at 950 °C for 90 min. Fig. 7(a) shows that the surface appears relatively smooth with only minor irregularities. The cross-sections shown in Fig. 7(a1, a2 and a3) illustrate the internal microstructure in different directions. The porosity is visible as dark spots within the material. The distribution of the pores appears to be relatively uniform in the different directions, with no significant orientation or alignment of the porosity. As can be seen in Fig. 7(b), there was a visible crack on the surface, suggesting that the reaction induced stresses within the pellet that led to fracture. The cross-sections shown in Fig. 7(b1), (b2) and (b3) reveal changes in the internal microstructure after the reaction. The pores appear to be larger and show an increased tendency to coalesce, especially in Fig. 7(b1) and (b2).

Fig. 8 shows the microtomographic images of a medium-sized pellet, comparing the microstructures during direct reduction at 950 °C for 90

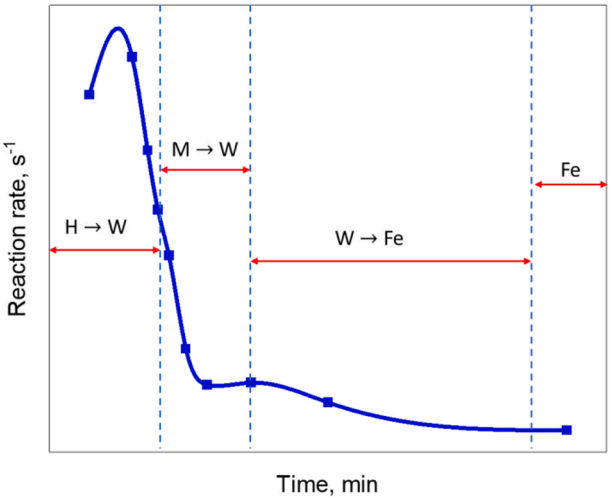

Fig. 5. Schematic of the reaction rate versus time for estimating the extent of H (H), M (M) to wustite (W), and wustite to Fe and Fe during the direct reduction of the pellets.

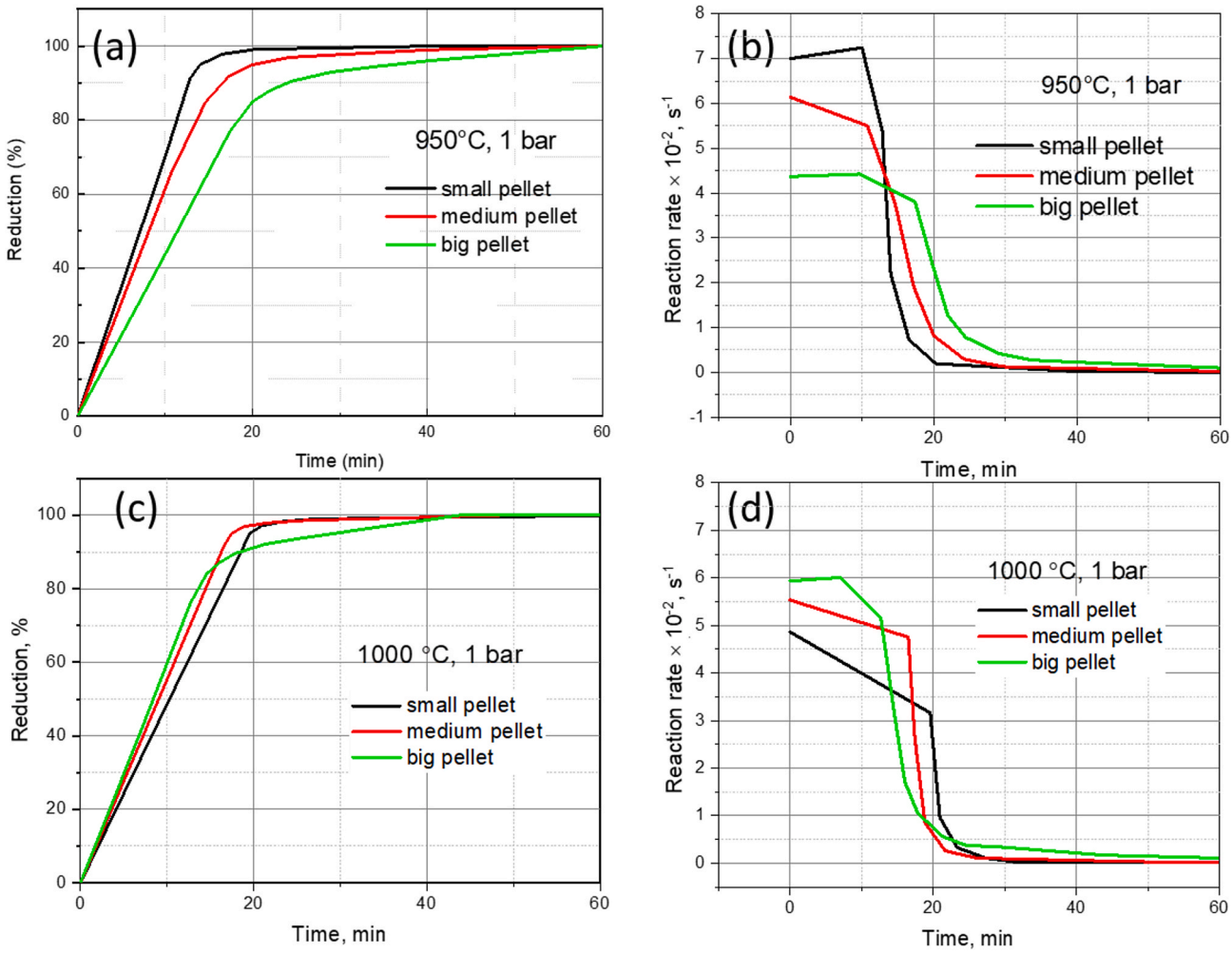

Fig. 6. (a,c)The reduction degree and (b,d)reaction rate as function of time at (a,b)950 °*C* and (c,d) 1000 °*C*.

Table 5
The estimated reduction rates for each reaction at 950 °*C* and 1000 °*C*. These rate values were extracted from Fig. 6.

Pellet	Reaction	Reduction rate × 10^{-2}, s^{-1}	
		950, °C	1000, °C
Small	H → M	7.2	4.26
	M → W	5.59	3.69
	W → Fe	0.79	2.91
Medium	H → M	7.1	5.21
	M → W	3.8	5.11
	W → Fe	0.65	3.31
Big	H → M	4.41	5.39
	M → W	2.65	5.04
	W → Fe	0.56	2.54

[a]H (H), M (M), wustite (W), and Fe.

min. Compared to the small pellets, both the small and the medium pellets have relatively smooth surfaces with minor irregularities in the unreduced state. In the reduced state, the small pellet developed a crack, while the medium pellet (Fig. 8 (b)) also showed surface changes, with the appearance of more pronounced deformations and roughness, although a clear crack was not as obvious as in the small pellet. In terms of porosity development, the porosity of the small pellet was evenly distributed in all directions in the unreduced state. After reduction, the porosity appeared to grow together, especially in the X and Y directions. The porosity of the medium pellet was also relatively uniform in the unreduced state. In the reduced state, the porosity was slightly larger and there were signs of coalescence, but not as pronounced as in the small pellet. The porosity in the reduced state of the medium pellet appeared to be more evenly distributed and the overall increase in pore size was less dramatic.

Fig. 9 shows microtomographic images of a large pellet before (unreduced state, images a-a3) and after (images b-b3), direct reduction at 950 °C for 90 min. In comparison with the previously provided images of the small and medium pellets, it can be seen that the external morphology of the small, medium and large pellets in the unreduced state has smooth surfaces with few features. The large pellet in Fig. 9 (a) appears to be similar to the medium and small pellets before reduction, with some surface roughness and irregularities. In the reduced state, the large pellet in Fig. 9 (b) has a cracked and deformed surface, similar to the medium pellet but more pronounced than the small pellet. In addition, the porosity distribution in the unreduced state was relatively evenly distributed across the X, Y and Z cross-sections for all pellet sizes. It should be noted that all pellets underwent changes in porosity after reduction. The small pellets showed a marked increase in pore size and connectivity, while the medium sized pellets showed increased porosity, with some signs of coalescence. The large pellet in Fig. 10 also showed an increase in porosity and coalescence in the cross-sections (b1, b2, b3), with the pores becoming more prominent and linear features forming that could indicate cracking. Therefore, cracking was observed in all pellet sizes after reduction.

Figs. 10–12 show microtomographic images of a small, medium and large pellet showing its morphology and internal structure before and